Continental Shelf Research 161 (2018) 49–57

Contents lists available at ScienceDirect

Continental Shelf Research

journal homepage: www.elsevier.com/locate/csr

Use of the Cone Penetration Testing (CPT) method to interpret late Quaternary tide-dominated successions: A case study from the eastern China coastal plain

Xia Zhang[a,*], Chun-Ming Lin[a], Robert W. Dalrymple[b], Shu Gao[c], Daniel T. Canas[b]

[a] State Key Laboratory for Mineral Deposits Research, School of Earth Sciences and Engineering, Nanjing University, 210023, China
[b] Department of Geological Sciences and Geological Engineering, Queen's University, Canada K7L3N6
[c] State Key Laboratory for Estuarine and Coastal Research, East China Normal University, 200062, China

ARTICLE INFO

Keywords:
Cone penetration test
Facies classification
Sequence-stratigraphic surface identification
Tide-dominated deposits
Late Quaternary
Eastern China coastal plain

ABSTRACT

We evaluate the applicability of cone penetration testing (CPT), calibrated using adjacent cores, as a tool for the sedimentological and stratigraphic examination of late Quaternary tide-dominated successions in the eastern China coastal plain. The results indicate that the sedimentary facies and sequence-stratigraphic surfaces can be readily distinguished using CPT profiles in the Qiantang River incised-valley system because of their distinctive mechanical behavior. The lithologic character of the various facies, which is controlled mainly by sediment supply, dynamic processes and post-depositional diagenesis, is the key factor affecting how well the CPT technique works. Within this particular macrotidal environment, which is dominated by non-cohesive sand and silt in the tidal channels, the accumulation of fluid mud is rare. Consequently, the tidal-channel deposits exhibit the geotechnical properties of coarse-grained sediments, and can be easily distinguished from the mud-dominated facies. However, in the nearby Changjiang delta system which is characterized by very high suspended-sediment concentrations and an abundance of fine-grained cohesive sediments, the presence of channel-bottom fluid muds makes it difficult to recognize channel deposits, because of the lack of a sharp lithologic contrast at their base. Consequently, the CPT method might not be as universally effective in tide-dominated systems as it appears to be in wave-dominated settings. Care is needed in the interpretation of the results from tide-dominated successions because of the widespread presence of fluid muds, the heterolithic nature of tidal deposits, the rheological similarity between adjacent facies, and the averaging of geotechnical properties between the alternating finer and coarser layers.

1. Introduction

The cone penetration testing (CPT) method, usually applied to foundation engineering investigations, has become increasingly popular in the sedimentological study of shallow, loosely-consolidated sediments in alluvial plains and coastal areas, because it provides in situ high-resolution information on the subsurface lithological succession with great accuracy and repeatability through direct comparison with the stratigraphy in adjacent cores (Robertson et al., 1986; Lunne et al., 1997; Tillmann et al., 2008; Robertson, 2009). In particular, it is portable, fast and economical, facilitates the automation and computerized management of data due to the adoption of digital electrical measurements, and does not need extensive coring. Consequently, this technique is significantly more convenient than traditional methods such as the collection of numerous cores and geophysical surveys (cf. Li and Lin, 2010; Lin et al., 2010).

Based on these advantages, CPT has been applied successfully to characterize the sedimentary facies, correlate subsurface stratigraphy and identify the key sequence-stratigraphic surfaces within Holocene successions along the northern margin of the Mediterranean Basin (Amorosi and Marchi, 1999; Lafuerza et al., 2005; Styllas, 2014). These systems are dominated by river flow and wave action, with minor tidal influence (Kapsimalis et al., 2005), which favours the effective separation of sand and mud into discrete sub-environments such that the deposits tend to be lithologically homogeneous, with clear geotechnical differences between the various facies.

In contrast, little work has been done to evaluate the utility of CPT profiles for the sedimentological study of tide-dominated systems, which are characterized by strongly heterolithic successions as a result of cyclic variations of tidal-current speed. In such successions, CPT

* Corresponding author.
E-mail address: zhangxiananjing@163.com (X. Zhang).

https://doi.org/10.1016/j.csr.2018.03.012
Received 9 June 2017; Received in revised form 19 December 2017; Accepted 30 March 2018
Available online 31 March 2018

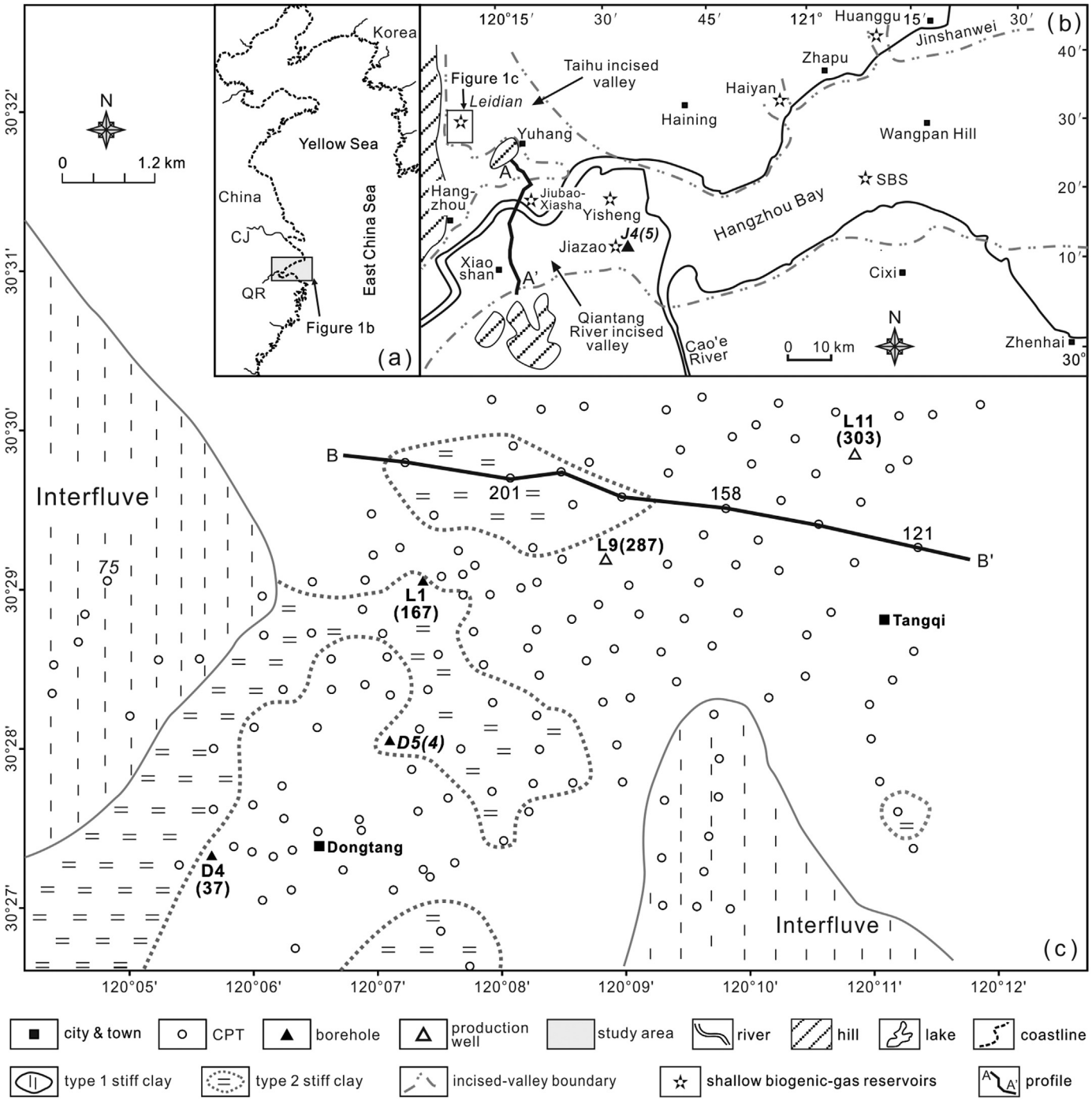

Fig. 1. (a) Map showing the general location of study area in eastern China. **(b)** Map of the modern Qiantang River estuary (see location in Fig. 1a) displaying the detailed location of the study area in the Taihu incised valley, a tributary of the main Qiantang River valley, and the locations of core J4, CPT-5, and profile A–A′ (modified from Lin et al., 2004, 2005; Zhang et al., 2013). **(c)** Map of the Leidian shallow biogenic-gas field (see location in Fig. 1b) showing the boundary of the postglacial Taihu incised valley, spatial distribution of the two different types of stiff clay, and the location of profile B–B′. Boldface lettering indicates the locations of cores and their associated CPT profiles (shown in parentheses). Italics are used to mark the CPTs and cores mentioned in this paper.

measurements can be significantly affected by sediment layering and the distance over which the cone averages the sediment resistance to cone penetration. This distance increases as the sediment stiffness increases (Lunne et al., 1997; Ahmadi and Robertson, 2005): it can be as small as 2–3 cone diameters (7.5–10 cm) in soft sediments, but up to 10–20 cone diameters (up to 75 cm) in stiff deposits. Thus, the sediment layering results in CPT values that are intermediate between those of the individual layers. Furthermore, clear lithologic and geotechnical distinctions do not always exist between the deposits of the different sub-environments in tidal systems, in particular because of the occurrence of fluid-mud deposits at the base of channels that would otherwise contain coarse-grained sediment (Schrottke et al., 2006; Dalrymple and Choi, 2007; Dalrymple, 2010; Feldman and Demko, 2015; Zhang et al., 2015, 2017).

The late Quaternary incised-valley successions underlying the modern Qiantang River estuary and the adjacent Changjiang delta in the eastern China coastal plain are tide-dominated systems (Fig. 1a; Li et al., 2002; Lin et al., 2005). Most of the sediment comprising the

succession beneath the coastal plain was supplied by the Changjiang (Yangtze River), one of the world's major rivers, that carries a very large load of fine-grained sediment (Shi et al., 2006; Zhang et al., 2014, 2017). Over the last 7000 yrs, approximately two thirds of the Changjiang-derived sediment has been deposited at its river mouth, but the remaining third is advected southward along the coast (Liu et al., 2007). Some of the well-sorted silty component of this sediment enters the Qiantang River estuary, which also receives dominantly sandy sediment supplied directly by the short Qiantang River (Sun et al., 1990; Lin et al., 2005; Wang, 2012; Yu et al., 2012; Xie et al., 2017). The facies characteristics and sequence-stratigraphic architecture of the two systems have been investigated previously using cores (Li et al., 2002; Lin et al., 2005; Zhang et al., 2014, 2017). In addition, ~ 500 CPT profiles (about 30–50 m penetration depth) were obtained in the course of an exploration program for shallow biogenic gas (Fig. 1b and c; Lin et al., 2004; Li and Lin, 2010; Zhang et al., 2013; Zhang and Lin, 2017), and the nearby cores enabled their lithologic calibration. The combination of these data sets provides a significant foundation for the present study, the aim of which is to evaluate the ability of CPT data to characterize the facies and identify key stratigraphic surfaces in tide-dominated systems.

2. Facies and stratigraphic architecture of the postglacial tide-dominated systems in the eastern China coastal plain

The Qiantang River incised valley, which was formed during the last sea-level lowstand, is located beneath the axis of the modern Qiantang River estuary (Fig. 1b). Its sediment fill is separated from the underlying basement by the sequence boundary (SB), which occurs as an undulating erosion surface that underlies the thalweg of the incised valley and extends up and out of the valley onto the interfluves (Lin et al., 2005; Zhang et al., 2014; Fig. 2a). From bottom to top, five facies associations (FA) are recognized within the valley fill: amalgamated fluvial channel (FA1) and floodplain and channel complex (FA2) that accumulated during the initial period of sea-level rise ~ 15,000–12,000 yr B.P., paleo-estuary (FA3; ~ 12,000–7500 yr B.P.), offshore shallow marine (FA4; ~ 7500–6000 yr B.P.) phase, and the modern estuary (FA5; 6000 yr B.P. to present; Zhang et al., 2014; Fig. 2a).

Stiff clay (FA6 or F1) occurs in two settings. The first (Type 1; F1-1) is widely distributed upon the interfluves, lying immediately below the SB (Fig. 2a). It is composed of mottled clayey silt, silty clay and clays, with abundant plant fragments, root traces, pedogenic voids and concretions, and vertical cracks that become wider upwards (Zhang et al., 2014). Consequently, it is interpreted to have resulted from long-term exposure of the interfluves from 25,000 yr B.P. to 12,000 yr B.P. (Chen and Li, 1998). It occurs at depths of 9.8–33.6 m, and is > 10 m thick (Fig. 2a). Stiff clay (Type 2; F1–2) also occurs in thinner intervals (1.0–4 m thick) within FA3 and FA5, where it was formed by relatively short-term exposure of the salt-marsh sediments in these units (Fig. 2b).

FA3 and FA5, the two main units of interest in this study, consist of tidal-channel (F2 and F5), tidal-flat and salt-marsh facies (F3, F6, and F7; Fig. 2b), and are characterized by the association of shallow- (e.g., *Ammonia beccarii* vars. and *Elphidium advenum*) and deep-water benthic foraminifera such as *Ammonia compressiuscula*, *Ammonia koeboeensis,* and *Ammonia ketienziensis* (water depths > 50 m). The tidal-channel facies (F2 and F5) is composed mainly of sediment ranging in size from silt to medium sand with relatively few (content < 30%), thin (1–2 mm thick) mud layers, and are characterized by an erosional base that is overlain by a fining-upward succession (Fig. 2b). The deposits of the tidal-flat and salt-marsh facies (F3, F6, and F7) are primarily composed of mud or sandy mud, intercalated with thin silt (0.1–2 cm thick) and shell-rich sand (8–20 cm thick) layers. The tidal-flat deposits can be easily differentiated from the salt-marsh sediments in FA5 but not in FA3, because of the lower content of silty layers and higher abundance of stiff clay within the salt-marsh sediments in FA5 (Fig. 2b).

The offshore shallow-marine deposits (F4; FA4) that are also the subject of this study consist mainly of soft mud (> 70% water content) with thin silt stingers (generally < 2 cm thick) and circular to elliptical silt bodies that fill burrows, and a high content of shallow-marine benthic foraminifera (e.g., *Ammonia beccarii* vars., *Elphidium magellanicum*, and *Cribrononion vetreum*).

In this succession, the initial flooding surface occurs within FA1 in the thalweg of the incised valley, and coincides with the SB on the interfluves (Fig. 2a). The maximum flooding surface lies within FA4 (Fig. 2a). The tidal ravinement and tidal erosion surfaces, formed by tidal-channel scour during transgression and progradation, respectively, are located at the base of FA3 and FA5 (Fig. 2a).

The late Quaternary Changjiang incised-valley fill consists of three main facies associations; from bottom to top they are amalgamated fluvial channel (deposited after the last glacial maximum and before 13,500 yr. B.P.), paleo-delta (13,500–9000 yr. B.P.), and modern delta (9000 yr. B.P. to present; Zhang et al., 2017). The paleo- and modern delta deposits can be further divided into five facies: tidal channel, tidal bar, tidal flat, salt marsh, and prodeltaic mud. Unlike the Qiantang River system, fluid-mud layers are abundant in the Changjiang succession, especially at the bottom of tidal channels, in the tidal-bar deposits of the delta front, and in the prodeltaic mud (Zhang et al., 2017).

3. CPT device and data interpretation

The CPT device (model number LMC-D130) used in this study was made by Liyang Keer Instrument Company Limited of Jiangsu Province, China. The CPT testing tool is composed of a double bridge probe located at the lower end of a succession of high-strength, stainless steel pipe segments, each of which is 1.0 m long, 38–42 mm in diameter and 6 mm thick (Li and Lin, 2010). The double bridge probe comprises a cone tip which was 10 cm^2 in basal area (3.57 cm in diameter) with an opening angle of 60° and a height of 3 cm, and a friction sleeve located behind the cone that had a surface area of 150 cm^2. These probe dimensions dictate that the thinnest homogeneous layer that can be distinguished in this study is 7.5–10 cm in soft sediments, but up to 75 cm for stiff deposits. The data-acquisition system included an analog to digital converter allowing the analog signals created by the cone tip and friction sleeve to be converted directly into potential-difference signals for storage on a computer for processing and plotting in real time (Li and Lin, 2010).

The double bridge probe and the metal pipes were pushed down into the sediment at a constant speed of 2 cm/s by the force of a push engine with thrust capacity of 20 t. As penetration progressed, two parameters, cone-tip resistance (q_c, in Mpa per unit area at the cone tip) and sleeve friction (f_s, in Mpa per unit area of the sleeve), were measured at 2 cm increments. Another parameter obtained is the friction ratio (FR, expressed in %), which is directly related to sleeve friction (Lafuerza et al., 2005):

$$\mathrm{FR}\ (\%) = f_s / q_c \times 100 \quad (1)$$

Based on these three parameters, the subsurface stratigraphy can generally be analyzed on site. Changes in q_c and f_s, and hence in FR, are interpreted as variations in the sediment type, because q_c is indicative of the soil density and consistency, and FR values represent variations in the grain size and sediment texture (Ahmadi and Robertson, 2005; Styllas, 2014). Generally, high q_c (> 8 MPa) and low FR (< 2%) values represent coarse-grained sandy sediment, whereas fine-grained silty and clayey deposits tend to have low q_c (< 4 MPa) and high FR (> 2%) values (Lunne et al., 1997). The most common chart used to estimate sediment types from CPT data is the one proposed by Robertson et al. (1986) which identifies 12 soil types by plotting q_c against FR (Fig. 3a). However, the fields in the Robertson et al. (1986) chart are intended to be accurate for burial depths of < 30 m; appropriate calibration should be made to account for the influence of overburden stress when using this chart to classify more deeply buried deposits. Fig. 3b shows,

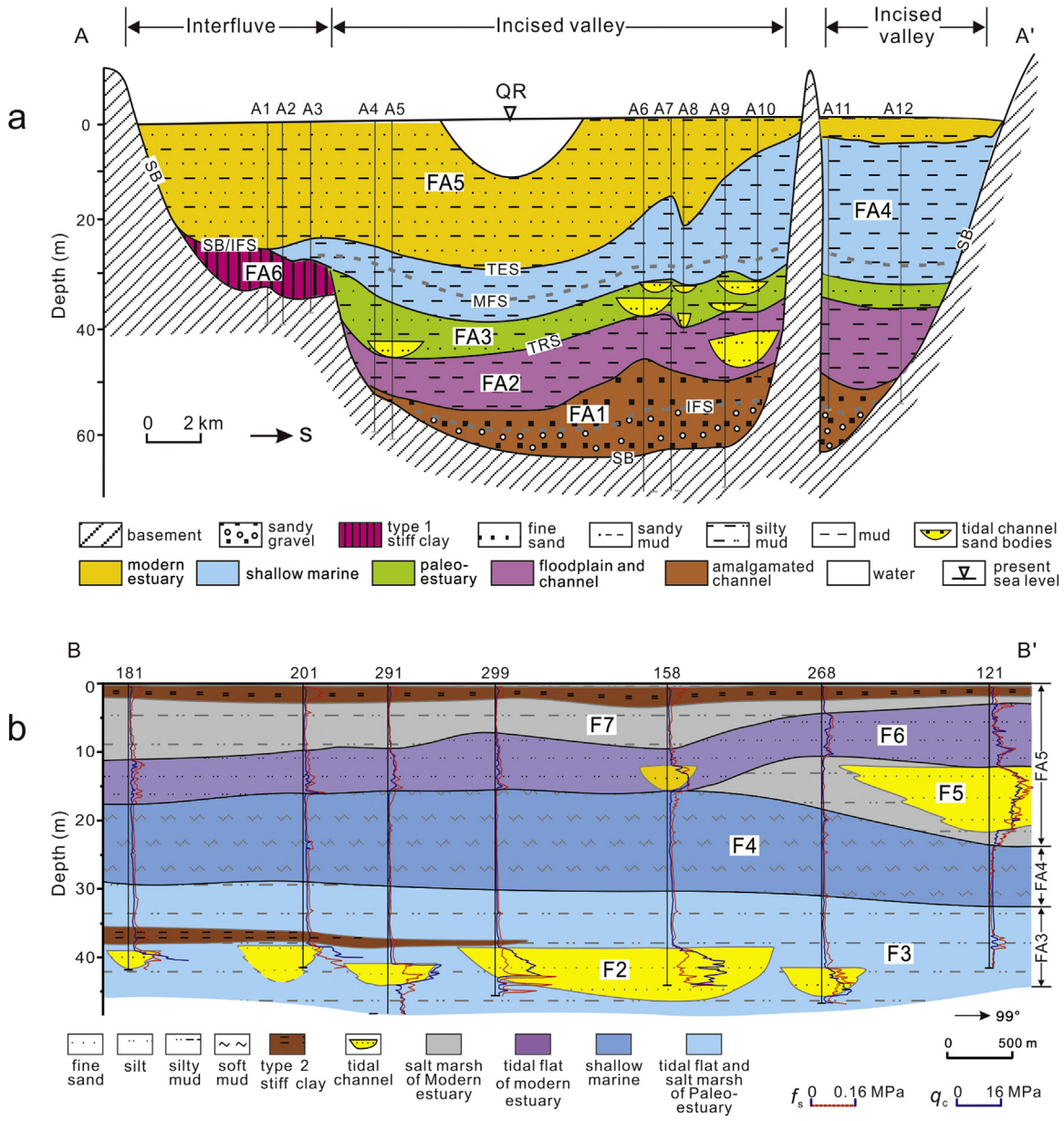

Fig. 2. (a) Stratigraphic transect A–A′ through the Qiantang River incised valley showing the distribution of major lithologies, facies associations (FAs), and key sequence-stratigraphic surfaces (modified from Zhang et al., 2015). See Fig. 1b for the location of profile A–A′. **(b)** Stratigraphic transect B–B′ in the Leidian shallow biogenic-gas field displaying the constituent facies of different facies associations and the distribution of Type 2 stiff clay. See Fig. 1c for the location of profile B–B′.

however, that any difference in consolidation that might have existed with increasing burial depth did not exert a significant influence on the geotechnical properties of the offshore shallow-marine mud (FA4), or on the properties of the tidal-flat and tidal-channel deposits in the paleo- and modern estuary (Table 1; Fig. 3a). Therefore, we have not calibrated our values for burial depth.

In this study, characterization of sedimentary facies was a stepwise process. The first step involved comparing the typical CPT profiles against nearby cores in order to establish the relationships between CPT parameters (q_c, f_s and FR) and the sedimentary facies recognized in the cores (see detailed facies characteristics in (Zhang, 2013) and (Zhang et al., 2014, 2017)), using the Robertson et al. (1986) chart (Fig. 3a). The second step was the interpretation and correlation of the remaining CPT profiles using the obtained relationships (Fig. 2b).

4. Results

Fig. 3a shows that the seven facies identified by core logging for the Qiantang River incised-valley succession (cf. Lin et al., 2005; Zhang et al., 2014) can be generally distinguished using the CPT technique, with each plotting in a different cluster on the Robertson et al. (1986) chart, with little or no overlap. On the whole, the seven facies plot within or close to the fields in which they might be expected to fall based on their lithology. However, the data for some environments (e.g., the modern tidal-channel facies; F5) depart from the field in which they might be expected to plot (fields 8 and 9; Fig. 3a) due to the common presence of muddy interlayers. Similarly, some generally muddy environments (e.g., modern tidal flats; F6) deviate toward more sandy fields (Fig. 3a) because of sandy interbeds. Overall, therefore, there is a tendency for the heterolithic nature of the deposits to expand the area in which each facies plots. It is also noteworthy that the stiff clay (F1), which has undergone moderate (F1–2) to significant (F1-1)

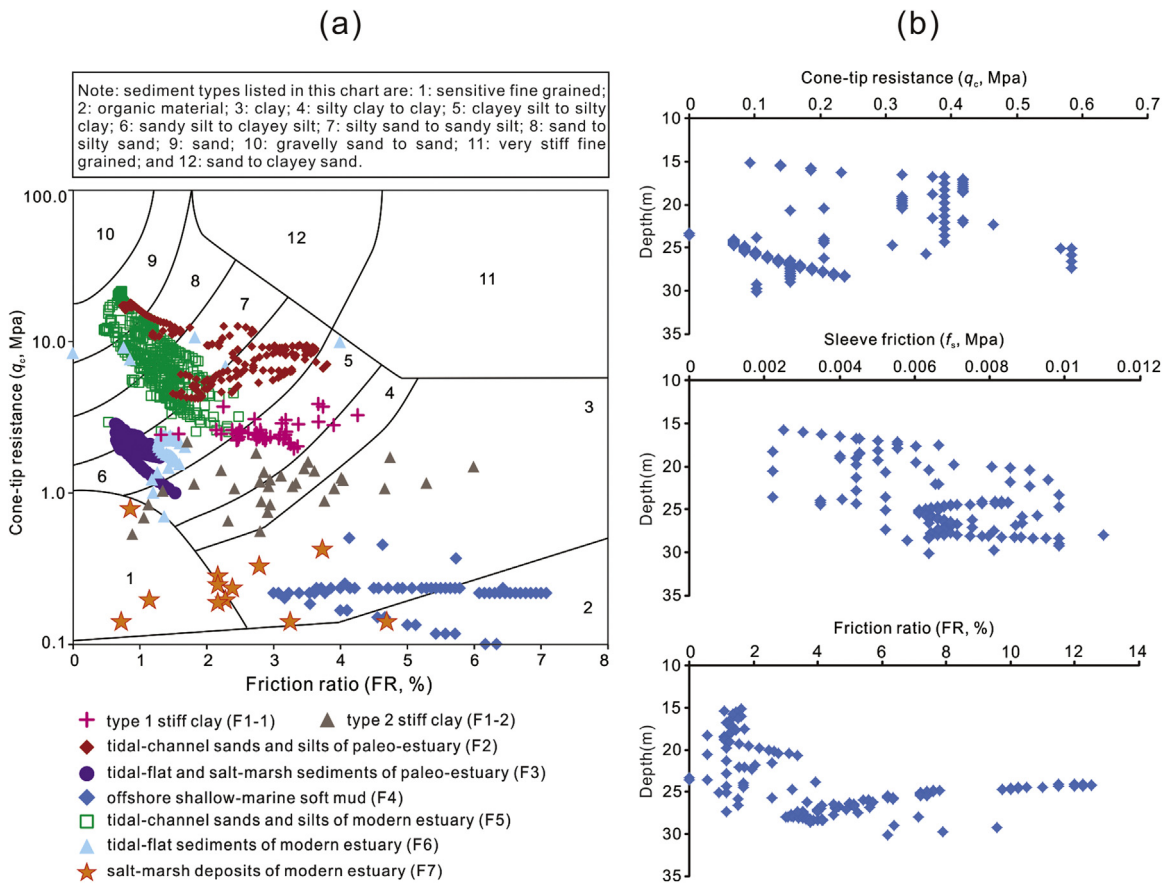

Fig. 3. (a) Plot of the different facies from the Qiantang River system on the Robertson et al. (1986) chart, after calibration between CPTs and adjacent cores. **(b)** Plots of the CPT parameters, q_c, f_s, and FR, of the soft mud in the offshore shallow-marine facies (F4) with burial depth indicating that no significant variation trend was detected for these CPT parameters with increasing depth.

levels of consolidation (see more interpretation in the Discussion section below) and might be expected to plot in or close to field 11, plots in areas that are more consistent with their original muddy lithology (i.e., fields 3–6), although with a distribution of data points that trends toward field 11 (Fig. 3a). This suggests that the stiff clays in the study area are not as consolidated as those used to construct Fig. 3a (Robertson et al., 1986).

Data points that fall in areas of overlap between clusters in Fig. 3a can be assigned to a particular facies by taking into account the depth in the profile at which the measurement occurs, which determines to which FA the points belong, and the shape of the CPT curves (Fig. 4a and b; Table 1). The tidal-channel sands and silts that occur in both the paleo- and modern estuary (i.e., F2 and F5, respectively) plot in fields 6–9 in Fig. 3a, and are characterized by an abrupt upward increase in the q_c and f_s values on CPT profiles, followed by a more gradual decrease caused by the upward-fining trend within the channel deposits (Fig. 4a; Table 1). Despite these similarities, F2 and F5 can be distinguished by their depths in the CPT profiles (Fig. 4a). However, in the nearby Changjiang incised-valley system, the tidal-channel facies present a very different, more complicated CPT profile, characterized by either a sharp decrease or increase at the channel base, followed by a upward increase and/or decrease in the CPT parameters, especially characterized by a sharp decrease in penetration resistance followed by a gradual increase (Fig. 4c). That occurs because of the accumulation of tide-generated fluid mud at the bottom of channels, which produces a channel succession that becomes more sand-rich upward above the channel base (cf. Zhang et al., 2017a; Dalrymple, 2010).

The fine-grained tidal-flat and salt-marsh deposits (i.e., F3, F6 and F7) in the paleo- and modern estuary exhibit gentle undulations on CPT profiles (Fig. 4a) and plot in fields 5–7 (Fig. 3a; Table 1), but they can be differentiated by taking into account the relative depth in the CPT profiles (Fig. 4a). It is worth noting that the tidal-flat and salt-marsh deposits in the paleo-estuary (FA3) are difficult to differentiate from each other using just the CPT profiles because of the similar lithology and small amount of Type 2 stiff clay in the salt-marsh facies in this unit.

The offshore shallow-marine deposits (F4), which plot in fields 2 and 3 (Fig. 3a), are marked by a very uniform cone-tip response that lies close to the baseline (Fig. 4a), as well as by the lowest q_c (0.07–0.25 MPa) and f_s (0.01–0.02 MPa) values, and the highest FR values (4.13–12.50%) of any of the deposits encountered (Table 1).

The stiff clay (F1) is typified by an abrupt increase in f_s values and a moderate increase of the q_c values relative to the over- and underlying fine-grained sediments, and mainly plots in fields 3–6 in Fig. 3a. Type 1 stiff clay (F1-1), present on the interfluves, is marked by high q_c (> 2 MPa) and f_s (> 0.06 MPa) values, and plots in fields 4–6 (Fig. 3a; Table 1). It exhibits a slightly wavy profile for both the q_c and f_s curves, and has an abrupt upper boundary (Fig. 4b). Type 2 stiff clay (F1–2), occurring in the paleo- and modern estuary (FA3 and 5), displays low q_c (< 2 MPa) and f_s (< 0.06 MPa) values (Table 1), plotting in fields 3–5 in Fig. 3a. The q_c curve is slightly undulatory and the f_s curve has the highest values in the middle of each occurrence, with a gradual decrease towards the top and bottom margins of occurrences (Fig. 4b; Table 1).

With regard to the recognition of the key sequence-stratigraphic surfaces within the Qiantang River incised-valley succession, the sequence boundary and initial flooding surface, which are represented by the top of the Type 1 stiff clay on the interfluves (Figs. 2a and 4b; Zhang et al., 2014), can be readily recognized as noted above, thereby permitting the incised-valley margin to be mapped (Fig. 1c). However, the

Table 1
Typical characteristics of CPT profiles for the major facies in the postglacial Qiantang River incised valley.

Facies	Characteristics of q_c and f_s curves	Value ranges q_c (MPa)	Value ranges f_s (MPa)	Value ranges FR (%)
F1–1: type 1 stiff clay (FA6)	Sharp contacts with the overlying sediments; a wavy linear shape for q_c and f_s curves	1.45–3.85/2.52(48)	0.03–0.14/0.07	1.31–4.28/1.31
F1–2: type 2 stiff clay (FA6)	Gradual contacts with the surrounding sediments; a slightly wavy q_c curve and a f_s curve has the highest f_s values in the middle	0.55–1.83/1.15(28)	0.01–0.09/0.04	1.12–5.99/3.27
F2: tidal-channel sands and silts in the paleo-estuary (FA3)	FU trends for q_c curves; large fluctuations with sharp peaks and troughs	5.52–29.39/12.24(153)[a]	0.11–0.33/0.20	0.72–3.80/2.05
F3: tidal-flat or salt-marsh clayey silt and silty clay of the paleo-estuary (FA3)	Smooth waveforms; pronounced fluctuations	1.58–6.06/2.46 (87)	0.01–0.10/0.03	0.63–1.84/0.92
F4: soft offshore shallow marine mud (FA4)	Approximate straight line, close to the baseline; minor fluctuations.	0.07–0.25/0.18(227)	0.01–0.02/0.01	4.13–12.50/6.47
F5: tidal-channel sands and silts of the modern estuary (FA5)	FU trend for q_c curves; sharp contact with the underlying sediments whereas gradational contact with overlying deposits; large fluctuations with sharp peaks and troughs	2.51–21.35/9.17(387)	0.05–0.16/0.10	0.46–2.48/1.22
F6: tidal-flat clayey silts and silty clays of the modern estuary (FA5)	Strongly fluctuating, in some places as gentle waveforms	0–2.39/1.89(66)	0–0.03/0.03	0.76–3.99/1.44
F7: salt-marsh clayey silts and silty clays of the modern estuary (FA5)	Approximate straight line, close to the baseline	0.09–0.78/0.19(24)	0–0.03/0.03	0.72–4.69/2.0

[a] 5.52–29.39/12.24 indicates the minimum-maximum/average values; numbers in parentheses indicate number of measured points; q_c = cone-tip resistance; f_s = sleeve friction; FR = friction ratio; FU = fining-upward trend.

sequence boundary and initial flooding surface which are located respectively at the bottom of and in the lower gravel sand part of the amalgamated fluvial channel facies association (FA1) within the incised valley (Fig. 2a) were not detected because the CPT tools did not penetrate through the gravels that comprise these deposits. Also, the CPT tools did not encounter the tidal ravinement surface, which is represented by the bottom of the paleo-estuary unit (FA3). The maximum flooding surface (MFS), that lies somewhere within FA4, also cannot be located precisely on CPT profiles because an obvious geotechnical contrast does not occur at this surface due to the relatively uniform nature of these muds, unlike the situation along the northern margin of the Mediterranean Sea where the MFS is indicated by the presence of a shell lag that is marked by a high q_c peak (Amorosi and Marchi, 1999; Lafuerza et al., 2005; Styllas, 2014). By contrast, the regressive, tidal erosion surface can be easily detected due to a prominent geotechnical contrast between the overlying tidal-channel sands and silts (F5) or tidal-flat silt and clay beds in the modern estuary (FA5) and the underlying softer offshore shallow-marine mud (FA4) (Figs. 2b and 4a). Nevertheless, this surface may be difficult to detect when the lithology of the tidal-flat or salt-marsh facies and offshore shallow-marine soft muds is similar, as shown by the CPT-268 profile in Fig. 2b.

5. Discussion

Based on the above analysis, the Robertson et al. (1986) chart supplemented by the relative depth in CPT profiles and the shape of the CPT curves is a relatively effective way to differentiate the major facies and identify key sequence-stratigraphic surfaces in the macrotidal Qiantang River incised-valley fill, a finding that is generally consistent with the previous work on depositional systems along the northern margin of the Mediterranean Sea (cf. Amorosi and Marchi, 1999; Lafuerza et al., 2005; Styllas, 2014). The main factor responsible for this result is the lithologic character of the deposits, which is in turn determined by the nature of the sediment supplied by fluvial and/or marine processes, the sediment dynamics, and the post-depositional processes (i.e., pedogenesis).

The Qiantang River incised valley is a macrotidal system and is, consequently, characterized by heterolithic stratification (Zhang et al., 2014), which might be expected to make lithologic differences between facies less distinct. However, the tidal-channel deposits, which are the most geotechnically distinctive facies, are sand-dominated with a sand content generally > 70%, even reaching 100%. Significantly, the mud layers that occur in these sands are generally only 1–2 mm thick and not particularly abundant (Zhang, 2013). Thus, they do not significantly influence the geotechnical parameters of the sands as recorded by the CPT device. Consequently, CPT profiles of the tidal-channel facies generally reflect the sandy nature of these deposits, plotting in fields 6–7 in Fig. 3a, especially in the lower part of channels, permitting the CPT technique to record the sharp erosional base, followed by the upward-fining trend that characterizes most channels (Fig. 4a).

This need not always be the case. In many tidal systems including the nearby Changjiang delta (Shen et al., 1992; Wu et al., 2012; Zhang et al., 2017; Fig. 4c), the Amazon River delta (Kineke et al., 1996), the Fly River delta (Dalrymple et al., 2003), and the Gironde and Severn estuary (Kirby and Parker, 1983), tide-generated fluid mud preferentially accumulates at the bottom of channels (Dalrymple et al., 2003; Ichaso and Dalrymple, 2009), leading to the generation of channel successions that become more sand-rich upward above the mud-dominated channel base (Dalrymple, 2010). In such cases, the CPT technique is less likely to detect the erosional base of the channel, as indicated by the example shown here from the Changjiang delta (Fig. 4c), even where it overlies muddy shallow-marine or tidal-flat deposits, because of the concentration of fluid-mud layers near the channel base.

The primary reason for the lack of fluid muds in the tidal-channel deposits of the Qiantang River system is sediment supply. It is well-

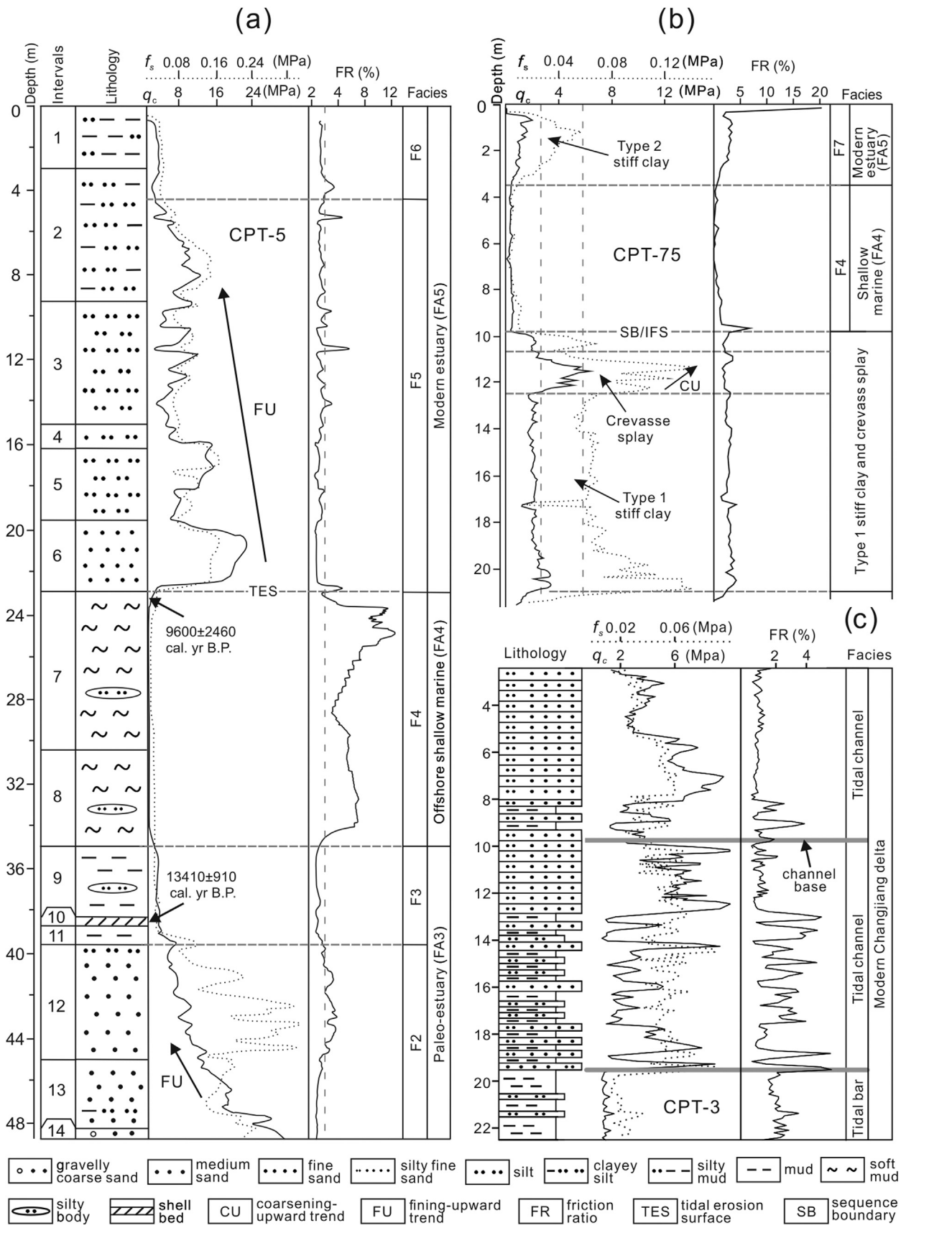

(caption on next page)

Fig. 4. (a) CPT-5 profile calibrated by the nearby core J4 (see location in Fig. 1b) and **(b)** CPT-75 profile (see location in Fig. 1c) showing the typical geotechnical features for the distinct facies identified in cores for the postglacial Qiantang River incised-valley system. See Fig. 3a for geotechnical values and legend of the facies. **(c)** CPT-3 profile calibrated by the nearby core ZK01 in the Changjiang incised-valley system displaying the characteristic geotechnical features of tidal channels with abundant fluid muds in the lower part of the channel. The distance between CPT profiles and the adjacent cores is generally less than 1 m. See detailed information on the sedimentary characteristics and AMS ^{14}C ages for core J4 in Lin et al. (2005), and core ZK01 in Zhang et al. (2017a). AMS ^{14}C ages reported in Lin et al. (2005) were recalibrated in this study using the method described in Zhang et al. (2015).

known that there are two main sediment sources for an estuary (sensu Dalrymple et al., 1992), namely the land via river discharge and seaward marine sources (cf. Dalrymple and Choi, 2007). The Qiantang River is a mountainous river that is 605 km long, with a drainage area of 48.8×10^3 km^2 (Zhang, 2013); as a result, it provides relatively sandy sediments to the coast. In addition, during the formation of the paleo-estuary (FA3; 12,000–7500 cal. yr B.P.), the Changjiang was apparently not exporting sand to the along-coast transport system, and was perhaps also exporting less mud than at present, because the river mouth lay nearly 200 km landward of its present exposed location (Zhang et al., 2015). As a result, flood-tidal currents and waves were able to rework previously deposited sand from the seaward extension of the Qiantang River incised valley and transport it landward into the paleo-estuary (Zhang et al., 2015). Consequently, there was abundant sand that accumulated in the tidal channels during the paleo-estuary phase. In the modern estuary (FA5), most of the sediment entering the system comes from the Changjiang and is carried landward by flood-tidal currents (Sun et al., 1990; Lin et al., 2005; Wang, 2012). These sediments consist predominantly of silt and very fine sand with a mean grain size > 80 μm (cf. Yu et al., 2012; Xie et al., 2017) that are easily resuspended and do not form fluid muds. In contrast, the suspended-sediment concentrations near the bed in the modern Changjiang delta are commonly very high, especially during the river flood period in the turbidity maximum zone, instantaneously reaching > 40 g/L, because of the huge content (> 95% of the total sediment load) of fine-grained sediments (< 63 μm) supplied by the river (Shi et al., 2006). This situation provides a favourable condition for the formation of fluid muds near the base of tidal channels (Zhang et al., 2017). Consequently, CPT is less likely to be effective in mud-dominated systems, and to work much better in sand-dominated tidal systems such as the modern Cobequid Bay-Salmon River estuary, Canada (Dalrymple and Zaitlin, 1994) and the Han River delta (Cummings et al., 2015) in which fluid mud is not abundant.

The tidal-flat, salt-marsh, and offshore shallow-marine deposits (F3, F4, F6, and F7) in the Qiantang River incised-valley system consist mainly of mud or sandy mud intercalated with thin silt and sand layers (0.1–2 cm thick; Zhang et al., 2014), due to the relatively lower energy setting in which they form compared to the tidal-channel deposits. The silt and sand layers within these facies are significantly thinner than the minimum thickness (7.5–10 cm) that can be distinguished by cone-tip resistance signals in this study. Thus, CPT profiles from these mud-dominated facies generally reflect their muddy nature and plot in fields 5–7 in Fig. 3a, resulting in a ready differentiation from the tidal-channel deposits (F2 and F5). Additionally, the tidal-flat and salt-marsh deposits (F3, F6, and F7) display a distinct CPT response compared to the offshore shallow-marine deposits (F4), as the former were deposited in a more energetic setting and contain a greater number of silt and sand layers. The cyclic variation of tidal-current speeds also generated cyclic variations in the abundance of the coarser-grained layers in the tidal-flat deposits, which causes the CPT profiles to be more irregular and to have overall higher q_c values than the shallow-marine sediments (Figs. 2b and 4; Table 1). However, when the lithology and, thus, the rheology of the tidal-flat and salt-marsh facies are similar, it is difficult to differentiate them.

Because of the pedogenesis which resulted in the over-consolidation and firm nature of the stiff clay, this sediment type behaves more like a coarse-grained soil, tends to dilate under shear, and has high undrained shear strength, causing an increase in q_c and f_s values relative to the unaltered sediment types (Fig. 3a; cf. Robertson, 2009). The most likely reason for the geotechnical differences between the two types of stiff clays is the coefficient of consolidation, which is in turn a result of differences in exposure time. F1-1, which mantles the interfluves, is interpreted to result from long-term (> 10 kyrs) exposure during the last sea-level lowstand (Chen and Li, 1998; Lin et al., 2005). This long-term pedogenesis caused the Type 1 stiff clay to become uniformly hard and over-consolidated to significant depths below the surface, forming an obvious contrast in geotechnical behavior with the overlying softer sediments, as was also found beneath the Venice lagoon, NE Italy (Tosi, 1994), and the southeastern Po Plain (Amorosi and Marchi, 1999). F1-1 is generally > 10 m thick, and thus, in most cases, the CPT device was unable to penetrate completely through it. Type 2 stiff clay (F1–2), by contrast, is thought to have formed as a result of shorter-term (decades to hundreds of years) exposure of fine-grained tidal-flat and salt-marsh deposits before sedimentation resumed (Dalrymple and Zaitlin, 1994), which caused F1–2 to be thinner and to have more gradational contacts with the over- and underlying deposits. The gradual increase and decrease of f_s values to a maximum in the middle of each occurrence most likely reflects a less consolidated upper part as a result of frequent wetting and drying, a more consolidated middle part because of downward translocation of clay minerals and precipitation of dissolved material, and a relatively less altered lower part (cf. Buol et al., 2011). Because of the thin nature and a lower degree of stiffness, CPT devices can pass through layers of F1–2.

6. Conclusions

The CPT technique, which has been successfully used in river- and wave-dominated settings to characterize sedimentary facies and identify key surfaces for sequence-stratigraphic analysis, may also have the potential to be applied to tide-dominated environments. The test reported here from the late Quaternary macrotidal Qiantang River incised-valley system indicates that CPT data can differentiate the seven facies and three key sequence-stratigraphic surfaces (SB, IFS and TES) recognized in cores, due to the distinct lithological compositions and geotechnical behaviours of the deposits of the various depositional sub-environments. However, settings that have the potential for the development of fluid mud (e.g., the Changjiang and other large deltaic systems) might generate successions in which the CPT technique will not yield sedimentologically meaningful results because of the concentration of such layers in the lower part of tidal-channel successions, thereby impacting the ability of the CPT technique to identify the channel floor. In addition, caution is required because of some other minor limitations in the interpretation of CPT data from tidal systems. First and most importantly, the heterolithic nature of tide-dominated deposits causes CPT data to have values that are intermediate between those of the individual layers because of the “averaging” of geotechnical parameters between layers. Secondly, this interlayering may also cause data points for each facies to occupy a larger area in the Robertson et al. (1986) than they would in a non-tidal system where such interlayering is not present. Thirdly, the rheological similarity of some facies may yield almost the same CPT profiles, causing non-unique facies interpretations. Greater care is needed in the interpretation of CPT data from tidal successions than from river- or wave-dominated environments.

Acknowledgements

This work is supported by the National Natural Science Foundation of China under Grant Numbers 41772097 and 41572112, and the Natural Science Foundation (Youth Science Fund Project) of Jiangsu Province (BK20140604). We thank C. W. Deng, J. Yu and J. Li for their assistance in field and core observations, sample analyses, and drafting. Thanks are also extended to C. Liu and C.S. Tang of Nanjing University for their helpful discussions and comments, and to Richard Brachman (Queen's University) for advice on the interpretation of CPT profiles. Special thanks are extended to the “Continental Shelf Research” Editor, Dr Andrea Ogston, and an anonymous reviewer for their constructive suggestions and comments.

References

Ahmadi, M.M., Robertson, P.K., 2005. Thin-layer effects on the CPT q_c measurement. Can. Geotech. J. 42, 1302–1317.

Amorosi, A., Marchi, N., 1999. High-resolution sequence stratigraphy from piezocone tests: an example from the Late Quaternary deposits of the southeastern Po plain. Sediment. Geol. 128, 67–81.

Buol, S.W., Southard, R.J., Graham, R.C., McDaniel, P.A., 2011. Soil Genesis and Classification, sixth ed. John Wiley & Sons, Inc, pp. 543.

Chen, Q.Q., Li, C.X., 1998. Studies on origin of the late Pleistocene stiff clays at the Yangtze delta. Sci. Geogr. Sin. 18, 53–57 (in Chinese with English abstract).

Cummings, D.I., Dalrymple, R.W., Choi, K., Jin, J.H., 2015. The Tide-Dominated Han River Delta, Korea: Geomorphology, Sedimentology, and Stratigraphic **Architecture**. Elsevier, Amsterdam, Netherlands, pp. 376.

Dalrymple, R.W., 2010. Tidal depositional systems. In: James, N.P., Dalrymple, R.W. (Eds.), Facies Models 4. St. John's, Geological Association of Canada, pp. 201–231.

Dalrymple, R.W., Baker, E.K., Harris, P.T., Hughes, M.G., 2003. Sedimentology and stratigraphy of a tide-dominated, foreland-basin delta (Fly River, Papua New Guinea). In: Sidi, F.H., Nummedal, D., Imbert, P., Darman, H., Posamentier, H.W. (Eds.), Tropical Deltas of Southeast Asia - Sedimentology, Stratigraphy, and Petroleum Geology 76. SEPM Spec. Publ., pp. 147–173.

Dalrymple, R.W., Choi, K., 2007. Morphologic and facies trends through the fluvial-marine transition in tide-dominated depositional systems: a schematic framework for environmental and sequence-stratigraphic interpretation. Earth-Sci. Rev. 81, 135–174.

Dalrymple, R.W., Zaitlin, B.A., Boyd, R., 1992. Estuarine facies models: conceptual basis and stratigraphic implications. J. Sediment. Petrol. 62, 1130–1146.

Dalrymple, R.W. and Zaitlin B.A., 1994. High-resolution sequence stratigraphy of a complex, incised valley succession, Cobequid Bay-Salmon River estuary, Bay of Fundy, Canada,Sedimentology, 41, pp. 1069–1091.

Feldman, H., Demko, T., 2015. Recognition and prediction of petroleum reservoirs in the fluvial/tidal transition. In: Ashworth, P.J., Best, J.L., Parsons, D.R. (Eds.), Fluvial-Tidal Sedimentology 68. Elsevier, Amsterdam, Netherlands, pp. 483–528.

Ichaso, A.A., Dalrymple, R.W., 2009. Tide- and wave-generated fluid mud deposits in the Tilje Formation (Jurassic), offshore Norway. Geol 37, 539–542.

Kapsimalis, V., Poulos, S.E., Karageorgis, A.P., Pavlakis, P., Collins, M., 2005. Recent evolution of a Mediterranean deltaic coastal zone: human impacts on the Inner Thermaikos Gulf, NW Aegean Sea. J. Geol. Soc. 162, 897–908.

Kineke, G.C., Sternberg, R.W., Trowbridge, J.H., Geyer, W.R., 1996. Fluid mud processes on the Amazon continental shelf. Cont. Shelf Res. 16, 667–696.

Kirby, R., Parker, W.R., 1983. Distribution and behavior of fine sediment in the Severn Estuary and inner Bristol Channel. U. K. Can. J. Fish. Aquat. Sci. 40, 83–95.

Lafuerza, S., Canals, M., Casamor, J.L., Devincenzi, J.M., 2005. Characterization of deltaic sediment bodies based on in situ CPT/CPTU profiles: a case study on the Llobregat delta plain, Barcelona, Spain. Mar. Geol. 222–223, 497–510.

Li, C.X., Wang, P., Sun, H.P., Zhang, J.Q., Fan, D.D., Deng, B., 2002. Late quaternary incised-valley fll of the Yangtze delta (China): its stratigraphic framework and evolution: sediment. Sediment. Geol 152, 133–158.

Li, Y.L., Lin, C.M., 2010. Exploration methods for late Quaternary shallow biogenic gas reservoirs in the Hangzhou Bay area, eastern China. AAPG Bull. 94, 1741–1759.

Lin, C.M., Gu, L.X., Li, G.Y., Zhao, Y.Y., Jiang, W.S., 2004. Geology and formation mechanism of late Quaternary shallow biogenic gas reservoirs in the Hangzhou Bay Area, Eastern China. AAPG Bull. 88, 613–625.

Lin, C.M., Zhuo, H.C., Gao, S., 2005. Sedimentary facies and evolution of the Qiantang River incised valley, eastern China. Mar. Geol. 219, 235–259.

Lin, C.M., Li, Y.L., Zhuo, H.C., Shurr, G.W., Ridgley, J.L., Zhang, Z.P., Xue, T., 2010. Features and sealing mechanism of shallow biogenic gas in incised valley fills (the Qiantang River, eastern China): a case study. Mar. Pet. Geol. 27, 909–922.

Liu, J.P., Xu, K.H., Li, A.C., Milliman, J.D., Velozzi, D.M., Xiao, S.B., Yang, Z.S., 2007. Flux, and fate of Yangtze River sediment delivered to the East China Sea. Geomorphology 85, 208–224.

Lunne, T., Robertson, P.K., Powell, J.J.M., 1997. Cone Penetration Testing in Geotechnical Practice. Blackie Academic, EF Spon/Routledge, New York.

Robertson, P.K., 2009. Interpretation of cone penetration tests - a unified approach. Can. Geotech. J. 46, 1337–1355.

Robertson, P.K., Campanella, R.G., Gillespie, D., Greig, J., 1986. Use of piezometer cone data. In: Clemence, S.P. (Eds.), In: Proceedings of the ASCE Specialty Conference In Situ'86: Use of In Situ Tests in Geotechnical Engineering, Blacksburg, Va., 23–25 June 1986. Geotechnical Spec. Publ. No. 6. New York, American Society of Civil Engineers (ASCE), pp. 1263–1280.

Shen, H.T., He, S.L., Pan, D.A., Li, J.F., 1992. A study of turbidity maximum in the Changjiang Estuary. Acta Geogr. Sin. 47, 472–479 (in Chinese with English abstract).

Shi, J.Z., Zhang, S.Y., Hamilton, L.J., 2006. Bottom fine sediment boundary layer and transport processes at the mouth of the Changjiang estuary, China. J. Hydrol. 327, 276–288.

Schrottke, K., Becker, M., Bartholoma, A., Flemming, B.W., Hebbeln, D., 2006. Fluid mud dynamics in the Weser estuary turbidity zone tracked by high resolution side-scan sonar and parametric sub-bottom profler. Geo-Mar. Lett. 26, 185–198.

Styllas, M., 2014. A simple approach to define Holocene sequence stratigraphy using borehole and cone penetration test data. Sedimentol 61, 444–460.

Sun, H.P., Li, C.X., Li, P., Tang, G.L., 1990. The tidal and sedimentary features of the lower reach of the Qiantangjiang River. Shanghai Geol. 9, 62–71 (In Chinese with English abstract).

Tillmann, A., Englert, A., Nyari, Z., Fejes, I., Vanderborght, J., Vereecken, H., 2008. Characterization of subsoil heterogeneity, estimation of grain size distribution and hydraulic conductivity at the Krauthausen test site using Cone Penetration Test. J. Contam. Hydrol. 95, 57–75.

Tosi, L., 1994. L'evoluzione paleoambientale tardo-quaternaria del litorale veneziano nelle attuali conoscenze. Quaternario 7, 589–596.

Wang, Y., 2012. Regional Oceanography of China Seas: Marine Geomorphology. Ocean Press, Beijing, pp. 371–377.

Wu, J.X., Liu, J.T., Wang, X., 2012. Sediment trapping of turbidity maxima in the Changjiang Estuary. Mar. Geol. 303–306, 14–25.

Xie, D.F., Pan, C.H., Wu, X.G., Gao, S., Wang, Z.B., 2017. The variation of sediment transport patterns in the outer Changjiang Estuary and Hangzhou Bay over the last 30 years. J. Geophys. Res. Oceans 122, 2999–3020.

Yu, Q., Wang, Y.W., Gao, S., Flemming, B., 2012. Modeling the formation of a sand bar within a large funnel-shaped, tide-dominated estuary: qiantangjiang Estuary, China. Mar. Geol. 299–302, 63–76.

Zhang, X., 2013. Sedimentary System of the Macrotidal-dominated Qiantang River Estuary and Incised Valley, Eastern China. Nanjing University, Jiangsu, China, pp. 153 (in Chinese with English abstract).

Zhang, X., Lin, C.M., Li, Y.L., Qu, C.W., Wang, S.J., 2013. Sealing mechanism for cap beds of shallow-biogenic gas reservoirs in the Qiantang River incised valley, China. Cont. Shelf Res. 69, 155–167.

Zhang, X., Lin, C.M., Dalrymple, R.W., Gao, S., Li, Y.L., 2014. Facies architecture and depositional model of a macrotidal incised-valley succession (Qiantang River estuary, eastern China), and differences from other macrotidal systems. GSA Bull. 126, 499–522.

Zhang, X., Dalrymple, R.W., Yang, S.Y., Lin, C.M., Wang, P., 2015. Provenance of Holocene sediments in the outer part of the Paleo-Qiantang River estuary, China. Mar. Geol. 366, 1–15.

Zhang, X., Dalrymple, R.W., Lin, C.M., 2017a. Facies and stratigraphic architecture of the late Pleistocene to early Holocene tide-dominated paleo-Changjiang (Yangtze River) delta. GSA Bull. 129. http://dx.doi.org/10.1130/B31663.1.

Zhang, X., Lin, C.M., 2017b. Characteristics and accumulation model of the late quaternary shallow biogenic gas in the modern Changjiang delta area, eastern China. Petrol. Sci. 14, 261–275.